WRC RESEARCH REPORT NO. 31

Microscopic Open Channel Boundary Layer Velocity Measurement Using a Virtual Image Method

Harry G. Wenzel
Assistant Professor of Civil Engineering

Kuo C. Chang
Research Assistant

T E R M I N A T I O N R E P O R T

Project No. A-026-ILL

The work upon which this publication is based was supported by funds provided by the U.S. Department of the Interior as authorized under the Water Resources Research Act of 1964, P.L. 88-379
Agreement No. 14-01-0001-1632

UNIVERSITY OF ILLINOIS
WATER RESOURCES CENTER
2535 Hydrosystems Laboratory
Urbana, Illinois 61801

April 1970

ABSTRACT

MICROSCOPIC OPEN CHANNEL BOUNDARY LAYER VELOCITY

MEASUREMENT USING A VIRTUAL IMAGE METHOD

A method for velocity measurement is described which employs a microscope and high speed motion picture camera to record the motion of small tracer particles suspended in the flow. The procedure, termed the image method, involves particle illumination such that the particle itself and its virtual image created by reflection from a boundary both appear on the film. The boundary is then located equidistant from the two images. The plane of focus is oriented normal to the boundary giving a picture of the entire velocity profile normal to the boundary within the limits of the field of view. A frame by frame analysis of the particle motion can yield velocity profile and turbulence information.

The image method was adapted to a small open channel. Considerable difficulty was encountered in illuminating the particles with sufficient intensity to impress their image on the film. Thus, quantitative data was not obtained. It was concluded that the lens system used to focus the light source was inadequate. However, the method has potential applications in velocity measurement near a boundary and flow visualization studies.

Wenzel, Harry G. and Chang, Kuo C.
MICROSCOPIC OPEN CHANNEL BOUNDARY LAYER VELOCITY
MEASUREMENT USING A VIRTUAL IMAGE METHOD
University of Illinois Water Resources Center Report No. 31
KEYWORDS--*boundary layers/ *microscopy/ open channel flow/
*tracers/ tractive forces/ *velocity measurement

ACKNOWLEDGEMENT

The project was under the direction of Professor Harry G. Wenzel, and the report was prepared in cooperation with Mr. Kuo C. Chang. In addition, Mr. Michael J. Mathews and Mr. Raymond E. Bradley were employed as research assistants during a portion of the project duration. The experimental work was performed in the Hydraulic Engineering Laboratory, Department of Civil Engineering.

CONTENTS

LIST OF FIGURES

LIST OF TABLES

NOTATION

D = diameter of field of view

F = free working distance of microscope lens

n_g, n_w = indices of refraction of glass and water

S = X coordinate of intersection of light ray with X axis

T = thickness of glass channel bottom

Δt = time increment

v = velocity

X, Y = coordinates of tracer particle

X_r, Y_r = coordinates of real image of particle

X_v, Y_v = coordinates of virtual image of particle

Z = distance from microscope lens to bottom of channel

β, Θ, ϕ = angles light rays make with the vertical

μ = micron

1. INTRODUCTION

1.1 — Objective and Scope

This report represents a continuation of the work which is described in WRC Research Report No. 13, "Microscopic Determination of Boundary Shear and Sublayer Turbulence Characteristics in an Open Channel"[1]*. The overall objective of these two studies is to develop and apply microscopic velocity measurement methods which would permit quantitative observation of the boundary layer region of an open channel. This information could then be used to investigate the local magnitude and distribution of boundary shear stress which in turn would permit a more intelligent design of channel geometry.

Basically the method involves the use of a microscope to observe the motion of small particles suspended in the flow. The particles are neutrally bouyant and are small enough so that they respond almost instantly to velocity fluctuations. Therefore, by photographing their motion using a high speed motion picture camera both local mean and turbulent velocity data can be obtained as described in Chapter 3.

The method described in WRC Report 13 was limited to observation of the particles in a plane which is parallel to the channel boundary Thus, in order to investigate variations normal to the boundary the plane of focus of the microscope must be adjusted to various distances from the boundary and data taken at each level. There are certain errors which are inherent to this method which exist because of the finite depth of focus of the objective lens of the microscope. These are discussed in detail in WRC Report 13. The method discussed in this report is based

---

*Raised numbers in parenthesis refer to reference list.

on a technique developed by Chen and Emrich[2] and Elrick and Emrich[3]. This technique, herein called the image method, involved the observation of particle motion in a plane which is normal to the boundary. The boundary is a plane reflecting surface and the light source is directed such that a direct or real image and a reflected or virtual image of a particle near the wall is seen and photographed through the microscope. The boundary is located, in general, midway between the images. Thus, this method gives a picture of the entire velocity profile normal to the boundary on one film since particles at various distances from the boundary appear on the film and the distance from the boundary of each particle can be directly measured. This procedure is a significant improvement over the previous one in that the errors associated with a velocity gradient existing across the depth of focus are generally eliminated because the principal velocity gradient is in the focal plane rather than across it.

This report describes the application of the image method to boundary layer velocity measurements in a small laboratory open channel. The apparatus is described and an analysis of the optics of the method is presented. A discussion of the advantages and disadvantages is given together with conclusions and recommendations.

1.2 — Review of Previous Study

The technique of flow visualization using a microscope was pioneered by Fage and Townend[4] who observed the particles present in ordinary tap water flowing in a square brass pipe. They employed a rotating lens system which permitted the observation of turbulent

velocity fluctuations but they were unable to obtain photographs. In 1936, Fage[5] reported observations of turbulent flow in a 1.064 in. diameter round tube. Again no photographs were taken. One year later, Vogelpohl and Mannesmann[6] published the results of quantitative velocity measurements in the laminar and transition region. A light interrupter disk was used to obtain streaks on a photograph and fine aluminum particles were used as tracers. Flow patterns were studied in the entrance and fully developed sections of a circular pipe. Fage has employed the ultramicroscope to make additional studies. In 1941, work with Preston[7] was reported in which the boundary layer transition from laminar to turbulent flow was studied. Again, in 1955, Fage reported additional studies of boundary layer flow[8].

Several more recent studies have resulted from a renewed interest in boundary layer flow and from the improvement of microscopic equipment. Bock[9] used polystrene latex spheres in a study of laminar flow in a small rectangular duct. He photographed their motion with a 35 mm camera, using a time exposure, to obtain streak photographs from which the velocity could be determined. Much of the microscopic equipment used in the present project is similar to that used by Bock. He made velocity measurements to within 10 microns (μ) of the boundary and verified the interesting and yet unexplained sinuous motion reported by previous investigators. The method was first used for open channel flow by Vasuki[10] who measured velocity profiles of laminar flow with depths of 80 to 120 μ. It was then adapted to turbulent open channel flow by Wenzel and Mathews[1]. Using equipment similar to Bock's Carver and Nadolink[11] measured velocity profiles of laminar flow of water in a rectangular tube with and without

non-Newtonian additives. They used a rotating disk to interrupt the light source, producing a series of streaks on 35 mm and Polaroid film. In subsequent work[12] they employed a 16 mm high speed camera to study laminar and turbulent velocity profiles of distilled water and aqueous solutions of non-Newtonian additives. It should be pointed out that all of the above studies were made using a real image method. That is the real image only of the particle was observed, a mechanical scheme was required to determine the distance from the boundary to the focal plane and the primary velocity gradient was normal to the focal plane.

The virtual image method was developed by Chen and Emrich[2] in boundary layer shock tube studies. It was then adapted to observation of the boundary layer region of a 1.52 in. by 0.567 in. rectangular pipe with air as the fluid and cigarette smoke particles as tracers.[3]

2. APPARATUS

2.1 — Flow System

The flow system was a modification of the apparatus described in WRC Report 13. The channel, shown inFig. 1 which was constructed inside the channel described in Report 13, was rectangular, 10 ft long, 1 in. wide with 1 in. side walls. The side walls were plexiglass and one wall was coated with a reflecting surface at the observation section. The channel itself was supported on an aluminum beam which can be seen in Fig. 1. The bottom of the channel rested on 6 in. by 10 in. glass support plates which in turn rested on pairs of adjusting screws which were threaded through the beam. The beam was pivoted at the downstream end and the slope could be adjusted by means of a screw system at the upstream end and read to 0.001 percent using a dial gage attached to the head tank. The water was recirculated using a 5 gpm centrifugal pump which was mounted in the floor and connected to the system through flexible hoses which prevented vibrations from being transmitted to the channel. Copper and vinyl tubing was used throughout. Flow rate was measured using a calibrated orifice meter, visible in Fig. 1, located in the return line below the beam.

Polystyrene laytex spheres supplied by Dow Chemical Company were used as tracer particles. The particles have a specific gravity of 1.05, an average diameter of 1.099 μ with a standard deviation of 0.0059 μ. About 15 drops of the 10 percent solid suspension was added to the 15 gal. of distilled water in the flow system, resulting in a final solid concentration of about 0.0025 percent.

2.2 — Microscope System

The microscope used was a commercial Leitz Laborlux II. It was mounted in an inverted position below the channel to eliminate the image refractions caused by small surface waves which would result in undesirable apparent particle motion. The microscope was mounted on a steel frame, shown in Figs. 1 and 2, which rested on the floor and was thus independent of the channel or camera. A view of the microscope in position with the camera removed is shown in Fig. 3. The focal point was adjustable by means of a micrometer screw calibrated in 1μ divisions. However, the calibration was not exact so a dial gage was mounted between the optical tube and the support beam as shown in Fig. 3. The gage was calibrated in 12.5μ divisions and could be interpolated to 2.5μ.

The optical system consisted of either a 32x or a 50x objective lens and a 10x eyepiece mounted in the optical tube. The depth of focal field of the 50x was experimentally determined to be about 11μ and that of the 32x was 24μ. It was concluded that the 32x lens was most appropriate since it produced a sharper image than the 50x. Its large depth of field was not a serious handicap.

The illumination system was the most critical part of the apparatus and proved to be the primary reason why quantitative data was not obtained. The light source was a 150 watt xenon lamp mounted on a frame above the channel as shown in Fig. 1. The light emitting from the lamp was focused through a lens system and reflected by a mirror shown in Fig. 4, down onto the channel. The mirror was set such that the axis of the light rays was slightly inclined to the vertical axis

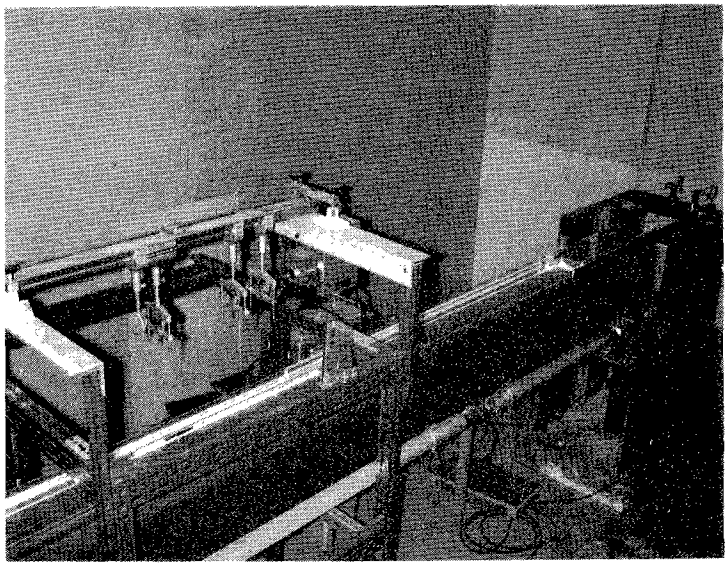

Fig. 1 — Channel and Illumination System

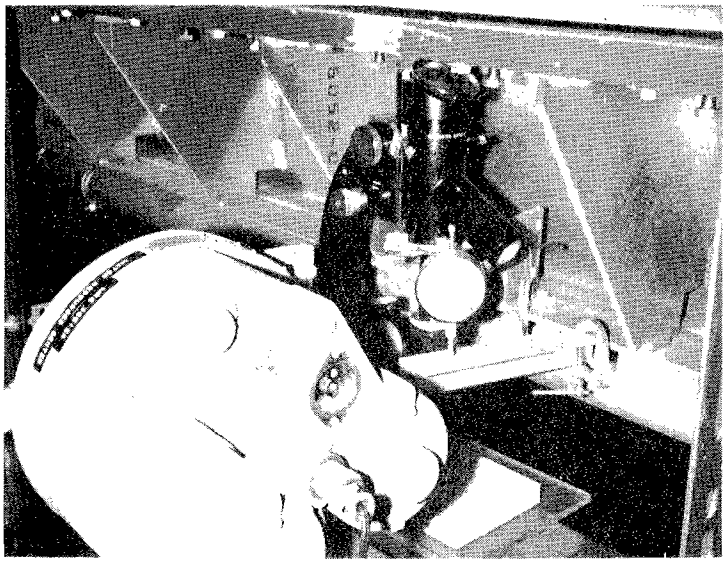

Fig. 2 — Microscope and Camera

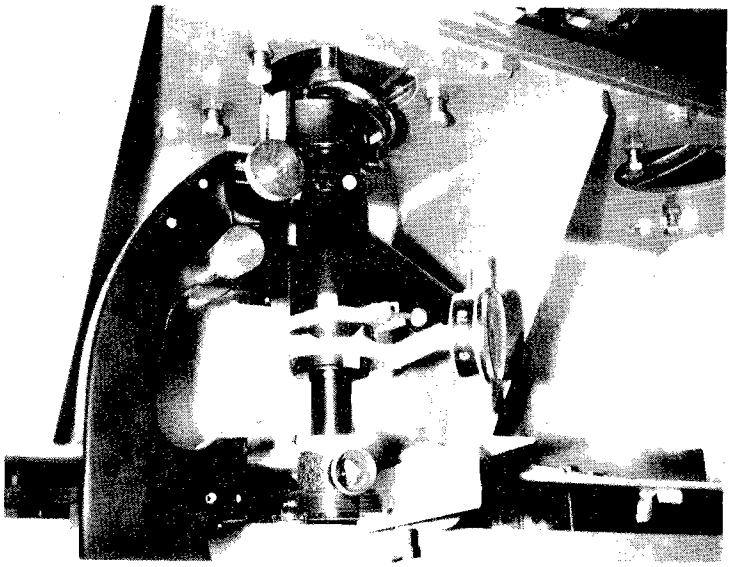

Fig. 3 — Microscope in Position Below Channel

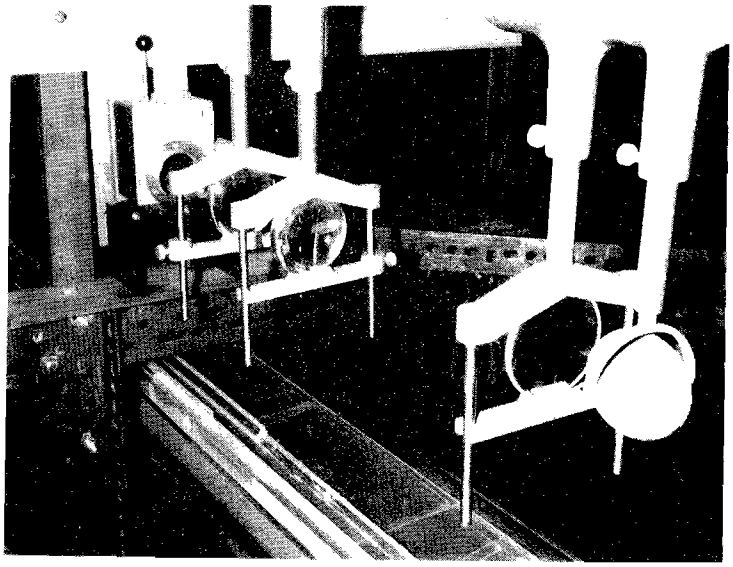

Fig. 4 — Xenon Light Source and Lens System

of the objective lens. This produced a dark field of view with only the light reflected by the particles passing into the lens. The light beam axis was also slightly inclined to the plane of the reflecting channel wall, thus producing a reflected as well as a real image. The mirror and lens were adjusted such that the light rays were focused at the desired point in the flow.

Particle motion was photographed with a 16 mm Fastax high speed motion picture camera, shown in Fig. 2, with a 100 ft film capacity and a 50 mm lens. The camera was mounted on a tripod and driven by a control unit. The particle image was transmitted into the lens through a lateral observation tube containing a deflecting prism and observed through the camera viewing system. The camera lens was positioned very closed but not in contact with the observation tube, thereby preventing camera vibrations from being transmitted to the microscope. Camera speeds of 1000 to 5000 frames/sec were used. To provide a fixed reference system on the film a cross-hair disk was mounted in the microscope tube. The cross-hair was aligned parallel and normal to the channel center line. Use of the cross-hair reference system would eliminate any errors due to camera vibration. A 1000 cycle/sec timing pulse was imposed on the edge of the Kodak Tri-x 16 mm negative film. The high frequency pulse was required since the film was constantly being accelerated as it was exposed causing the time interval between frames to vary.

2.3 — Experimental Procedure and Data Reduction

Because of lighting problems, as discussed later in the report, none of the film which was taken was analyzed frame by frame. However,

the experimental procedure and data reduction method are well developed and are described in detail in WRC Report 13. Only a brief summary is presented here.

After the desired flow conditions were achieved and recorded, the microscope was focused so that the channel bottom was near the upper limit of the plane of focus. This was used as the zero depth position and the dial gage and micrometer adjusting screw position on the microscope was noted. The microscope was then raised a predetermined distance using the micrometer screw, and its reading as well as that of the dial gage were recorded. The lens and mirror system was adjusted for optimum contrast. A 100 ft spool of film was then placed in the camera, the desired speed set on the camera control unit, and the film exposed. A length scale was established by photographing a stage micrometer which was divided into 10μ increments.

The data reduction procedure as followed in Report 13 consisted of three phases: (a) determination of a real time calibration of the film on a frame by frame basis, (b) establishment of the coordinates of the particles judged to be in focus, and (c) computation of the velocity of each particle between two successive frames.

The time calibration was based on the 0.001 sec timing marks on the film edge. The film was projected on a screen and the position of each mark was correlated with frame number. Through the use of a computer program the calibration was smoothed and transformed into a time associated with the beginning of each frame.

It was planned to obtain particle coordinates using a Wild STK-1 Optical Comparator which was available. This instrument is capable of recording an unmagnified length to within 1μ. Particle and cross-hair

coordinates could be recorded directly on computer cards along with frame number.

A computer program was available to use the above data to compute particle velocities using the general equation $v = \Delta x/\Delta t$ where Δx is the difference in coordinates of a particle in either the longitudinal or lateral directions during a time interval Δt. With particle velocity computations complete mean velocity profiles, boundary shear, and turbulence parameters can be computed.

3. ANALYSIS OF THE IMAGE METHOD

3.1 — Location of Virtual Image of Particle

As described in Chapter 1, the image method produces a picture of particle motion in a plane normal to a reflecting boundary. Both a real and virtual image is seen. In order to determine the location of the particle with respect to the boundary an analysis of light ray patterns is useful.

Referring to Fig. 5, two light rays, R_1 and R_2, reflecting from the particle P are shown. The rays reflect off the vertical reflecting channel wall and pass through the glass bottom of thickness T, into the air and finally into the microscope objective lens. The purpose of the following development is to determine expressions for the coordinates of the virtual image, (X_v, Y_v), in terms of the actual coordinates of the particle (X, Y) and the angles shown. The cartesian coordinate system is set with the axes coinciding with the vertical reflecting wall and the top surface of the glass bottom. The virtual image will be located at the intersection of the dashed lines which are extrapolations of the rays back at the angels ϕ_1 and ϕ_2. From Fig. 5 the following expressions can be written.

$$\tan \phi_1 = \frac{S_1 + \Delta S_1 - X_v}{Y_v + T} \qquad (1\text{-a})$$

$$\tan \phi_2 = \frac{S_2 + \Delta S_2 - X_v}{Y_v + T} \qquad (1\text{-b})$$

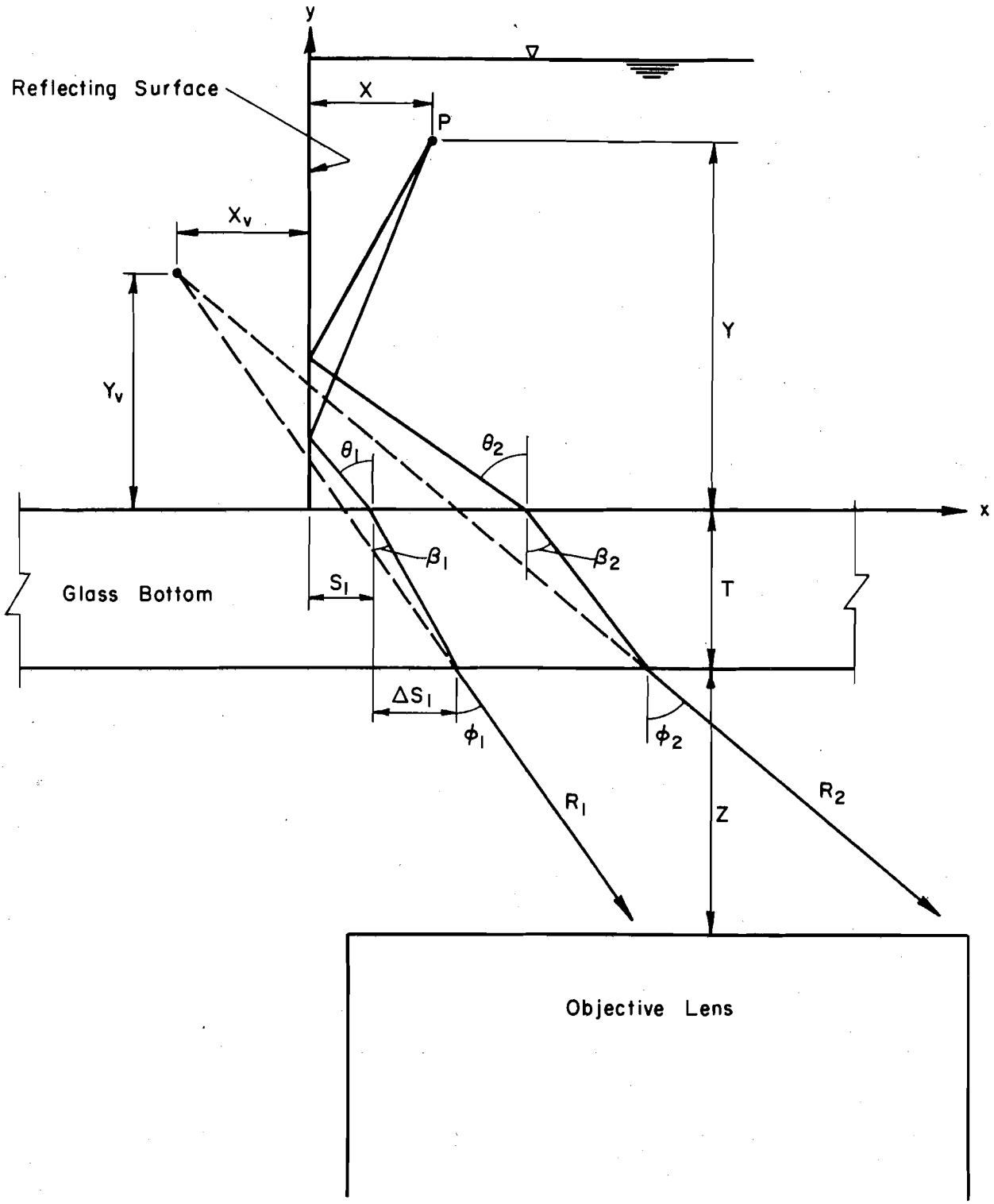

FIG. 5 RAY PATTERNS FOR VIRTUAL IMAGE

where S is the x coordinate of the intersection of a ray with the x axis and ΔS is the change in the x coordinate as the ray passes through the glass. Solving Eqs. 1 simultaneously

$$X_v = \frac{\tan\phi_2 \ (S_1 + \Delta S_1) - \tan\phi_1 \ (S_2 + \Delta S_2)}{\tan\phi_2 - \tan\phi_1} \tag{2-a}$$

$$Y_v = \frac{(S_2 + \Delta S_2) - (S_1 + \Delta S_1)}{\tan\phi_2 - \tan\phi_1} - T \tag{2-b}$$

The following relationships are needed. In general

$$\Delta S = T\tan\beta = \frac{T\sin\beta}{(1 - \sin^2\beta)^{1/2}} \tag{3}$$

From Snell's law

$$\frac{\sin\theta}{\sin\beta} = \frac{n_g}{n_w} \tag{4}$$

where n_g and n_w are the refractive indices of glass and water respectively. Therefore

$$\Delta S = \frac{T\frac{n_w}{n_g}\sin\theta}{\left[1 - (\frac{n_w}{n_g}\sin\theta)^2\right]^{1/2}} \tag{5}$$

Also from Snell's law

$$\sin\phi = n_w \sin\theta \tag{6}$$

and thus

$$\tan\phi = \frac{\sin\phi}{(1 - \sin^2\phi)^{1/2}} = \frac{n_w \sin\theta}{\left(1 - (n_w \sin\theta)^2\right)^{1/2}} \tag{7}$$

Finally it is evident that

$$Y\tan\theta = S + X \tag{8}$$

Now substituting, with appropriate subscripts, Eqs. 5, 7, and 8 into Eqs. 2 and simplifying

$$X_v = \frac{Y\left[\sin\theta_2\tan\theta_1(1 - n_w^2\sin^2\theta_1)^{1/2} - \sin\theta_1\tan\theta_2(1 - n_w^2\sin^2\theta_2)^{1/2}\right]}{\sin\theta_2(1 - n_w^2\sin^2\theta_1)^{1/2} - \sin\theta_1(1 - n_w^2\sin^2\theta_2)^{1/2}} - X$$

$$+ \frac{Tn_w\sin\theta_1\sin\theta_2\left[\left(\frac{1 - n_w^2\sin^2\theta_1}{n_g^2 - n_w^2\sin^2\theta_1}\right)^{1/2} - \left(\frac{1 - n_w^2\sin^2\theta_2}{n_g^2 - n_w^2\sin^2\theta_2}\right)^{1/2}\right]}{\sin\theta_2(1 - n_w^2\sin^2\theta_1)^{1/2} - \sin\theta_1(1 - n_w^2\sin^2\theta_2)^{1/2}} \tag{9-a}$$

$$Y_v = \frac{Y(\tan\theta_2 - \tan\theta_1)\left[(1 - n_w^2\sin^2\theta_2)(1 - n_w^2\sin^2\theta_1)\right]^{1/2}}{n_w\left[\sin\theta_2(1 - n_w^2\sin^2\theta_1)^{1/2} - \sin\theta_1(1 - n_w^2\sin^2\theta_2)\right]^{1/2}} - T$$

$$+ \frac{T\left[\dfrac{\sin\theta_2}{(n_g^2 - n_w^2\sin^2\theta_2)^{1/2}} - \dfrac{\sin\theta_1}{(n_g^2 - n_w^2\sin^2\theta_1)^{1/2}}\right]\left[(1 - n_w^2\sin^2\theta_2)(1 - n_w^2\sin^2\theta_1)\right]^{1/2}}{\sin\theta_2(1 - n_w^2\sin^2\theta_1)^{1/2} - \sin\theta_1(1 - n_w^2\sin^2\theta_2)^{1/2}} \qquad (9\text{-b})$$

It should be pointed out here that if the angles are small such that $\tan\theta \simeq \sin\theta$ and $\sin^2\theta << 1$ Eqs. 9 reduce to

$$X_v = - X \qquad (10\text{-a})$$

$$Y_v = \frac{Y}{n_w} - T\left(1 - \frac{1}{n_g}\right) \qquad (10\text{-b})$$

The equations for the coordinates of the real image (X_r, Y_r), referring to Fig. 6, are developed in the same manner except that Eq. 8 now becomes

$$Y\tan\theta = S - X \qquad (11)$$

This merely produces a change in the sign of the second term on the right side of Eq. 9-a and the final result corresponding to Eqs. 10 is

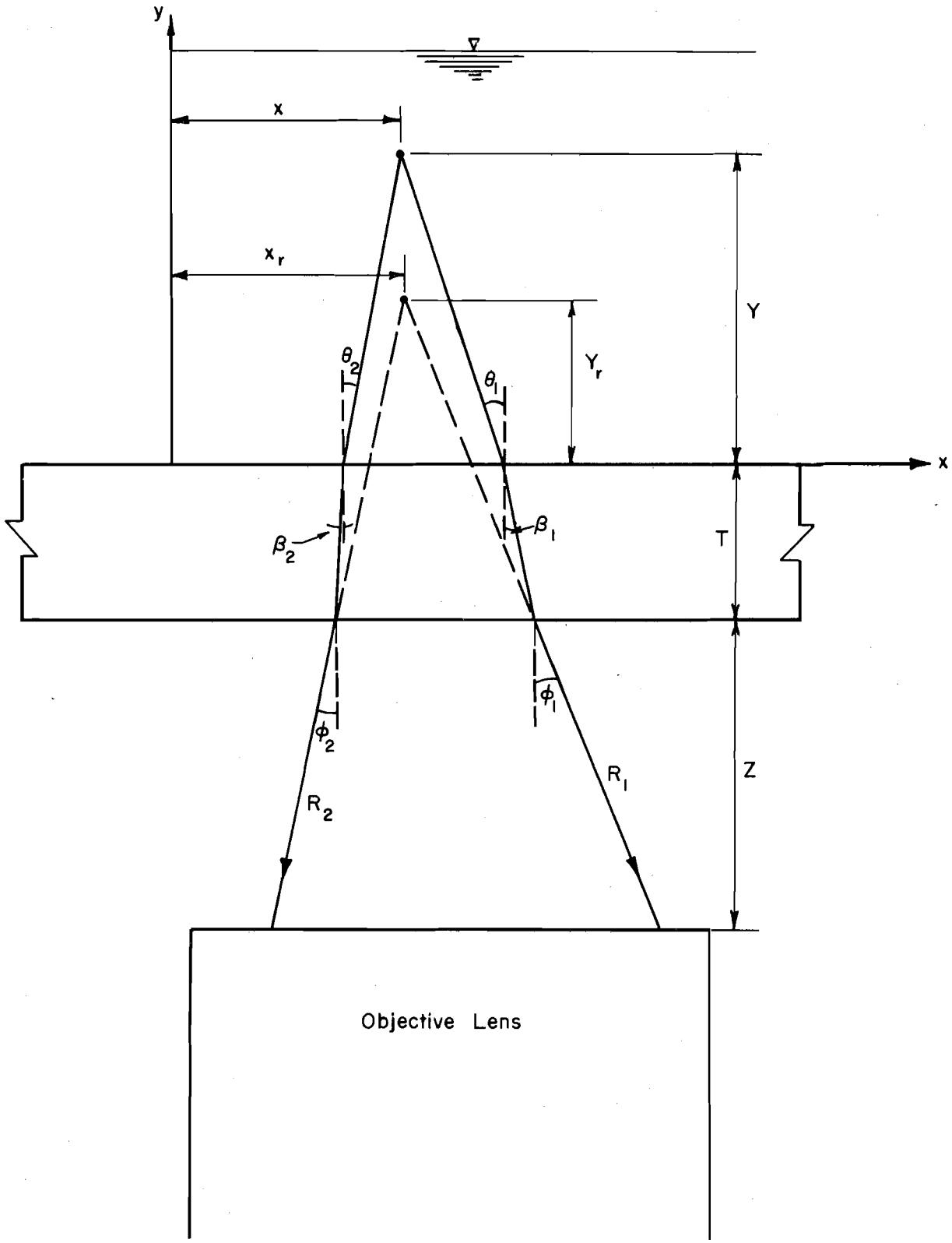

FIG. 6 RAY PATTERNS FOR REAL IMAGE

$$X_r = X \tag{12-a}$$

$$Y_r = \frac{Y}{n_w} - T\left(1 - \frac{1}{n_g}\right) \tag{12-b}$$

Thus, it is seen that if the small angle assumption is valid the real and virtual images are symmetrically located about the reflecting wall and the actual distance from the wall of the particle can be determined simply by dividing the scaled distance between the particles on the film in half.

In order to investigate the validity of the small angle assumption Eqs. 9 are modified to the limiting condition $\phi_1 \to \phi_2 \to \phi_{max}$ where ϕ_{max} is the maximum vertical angle with which a light ray can enter the objective and be transmitted through the microscope lens system. This angle was experimentally determined for each lens by viewing a stage micrometer and noting the diameter, D, of the field of view. Thus

$$\phi_{max} = \frac{D}{2F} \tag{13}$$

where F is the free working distance of the objective. Table 1 shows the result for the two lenses used.

Table 1. Objective Lens Properties

Lens	Numerical Aperture	F	D	θ_{max}	θ_{max}	Depth of Focal Field
32x	0.30	14,900μ	570μ	0.0269	0.0203	11μ
50x	0.60	6,500μ	350μ	0.0269	0.0203	24μ

It is seen that ϕ_{max} is small enough so that the approximation is valid for practical purposes. However, this can be further verified through the following development.

$$\sin\theta_2 = \sin(\theta_1 + \delta\theta) \simeq \sin\theta_1 + \delta\theta\cos\theta_1 \tag{14-a}$$

$$\tan\theta_2 = \tan(\theta_1 + \delta\theta) = \tan\theta_1 + \delta\theta \tag{14-b}$$

$$(1 - n_w^2\sin^2\theta)^{1/2} = 1 - \frac{n_w^2\sin^2\theta}{2} + \frac{3}{8}(n_w^2\sin^2\theta)^2 + \ldots \tag{14-c}$$

Using Eqs. 14-a, b, and the first two terms of the bionomial expansion in Eq. 14-c, can be simplified.

$$\sin\theta_2(1 - n_w^2\sin^2\theta_1) - \sin\theta_1(1 - n_w^2\sin^2\theta_2) \simeq \delta\theta\cos\theta_1\left(1 - \frac{n_w^2}{2}\sin^2\theta_1\right) \tag{15-a}$$

$$Y \sin\theta_2 \tan\theta_1 (1 - n_w^2 \sin^2\theta_1)^{1/2} - Y \sin\theta_1 \tan\theta_2 (1 - n_w^2 \sin^2\theta_2)^{1/2} \simeq Y n_w^2 \delta\theta \sin^3\theta_1 \quad (15\text{-b})$$

$$T n_w \sin\theta_1 \sin\theta_2 \left[\left(\frac{1 - n_w^2 \sin^2\theta_1}{n_g^2 - n_w^2 \sin^2\theta_1} \right)^{1/2} - \left(\frac{1 - n_w^2 \sin^2\theta_2}{n_g^2 - n_w^2 \sin^2\theta_2} \right)^{1/2} \right] \quad (15\text{-c})$$

$$\simeq \frac{T n_w n_g \delta\theta \sin^3\theta_1 \cos\theta_1 (n_w^2 - \frac{n_w^2}{n_g^2})}{n_g^2 - n_w^2 \sin^2\theta_1}$$

Substituting Eqs. 15 into Eqs. 9, dropping the subscript on θ and simplifying

$$X_v = \frac{Y \tan\theta \sin^2\theta n_w^2}{1 + \frac{n_w^2}{2} \sin^2\theta} + \frac{T n_w^3 n_g \sin^3\theta (1 - \frac{1}{n_g^2})}{(n_g^2 - n_w^2 \sin^2\theta)(1 + \frac{n_w^2}{2} \sin^2\theta)} - X \quad (16\text{-a})$$

$$Y_v = \frac{y(1 - n_w^2 \sin^2\theta)}{n_w (1 + \frac{n_w^2}{2} \sin^2\theta) \cos\theta} + \frac{T n_g (1 + \frac{n_w^2}{2n_g^2} \sin^2\theta)(1 - n_w^2 \sin^2\theta)}{(1 + \frac{n_w^2}{2} \sin^2\theta)(n_g^2 - n_w^2 \sin^2\theta)} - T \quad (16\text{-b})$$

Furthermore it can be seen from Fig. 5 that the limiting condition such that $\phi \rightarrow \phi_{max}$ corresponds to a particle at its maximum visible distance

from the vertical wall

$$X = Y \tan\theta \tag{17}$$

Eq. 16-a, using Eq. 17, was used to show the maximum percent difference between X and X_v as a function of θ, T and Y. Fig. 7 shows the effect of θ on the difference. It is seen that the angle is an important variable with the difference increasing approximately with the square of the angle and that the difference approaches a constant percentage as Y increases. The effect of T on the difference is shown in Fig. 8 which is for the two objectives described in Table.1. It is seen that as T increases the difference increases although it is not as sensitive to relative changes in T as is to relative changes in θ. Again as Y increases the difference approaches a constant percentage.

The effect of θ, T and Y on the difference between the Y coordinates of the real and virtual images is shown in Figs. 9 and 10. In Fig. 9, Eq. 16-b was evaluated for various depths and T values with the limiting θ from Table 1. The term Y_{vo} represents the value of Y_v for a particle at Y = 0. It is seen that the percent difference is greater than the corresponding X coordinate value and that it increases with increasing T. Fig. 10 shows the absolute value of the Y coordinate differences for each lens as a function of Y. This shows that the difference is less than the depth of focal field of either lens and so even for this extreme case the difference could not be easily detected.

Although the previous discussion was limited to dealing with rays entering the lens at the maximum permissable angle, in general rays of smaller angles are present. The general effect of the glass bottom,

then, is to cause the rays to focus over a region which is larger than the particle itself. This explains in part the fact that the particles appear larger on the film than their actual size. Defraction also contributes to this effect. However, the discussion shows that this enlargement is not significant. Fig. 11 shows an enlargement of a portion of a film which shows the particles and their virtual images.

3.2 — Limitations on Size of Viewing Field

The maximum depth, Y, above the channel bottom at which a particle can be seen is a function of the free working distance of the lens, F, as well as the thickness of the bottom glass. From Fig. 5, the distance from the objective to the image is made up of three components.

$$F = Z + T + Y_v \tag{18}$$

Solving for Z and substituting Eq. 10-b

$$Z = F - T\left[\frac{Y}{n_w} - T\left(1 - \frac{1}{n_g}\right)\right]$$

$$Z = F - \frac{Y}{n_w} - \frac{T}{n_g} \tag{19}$$

The maximum value of Y corresponds to Z = 0.

$$Y_{max} = n_w F - \frac{n_w}{n_g} T = 1.33F - 0.864T \tag{20}$$

Using values of F from Table 1 yields Y_{max} = 14,400μ for the 32X lens and Y_{max} = 2,160μ for the 50X lens.

The maximum value of X for which a virtual image can be seen is limited by the maximum visual angle θ_{max} as given in Table 1.

$$\tan\theta_{max} = \frac{X_{max}}{Y} \tag{21}$$

Since θ is small $\tan\theta_{max} = \sin\theta_{max}$ and using Eq. 6

$$X_{max} = \frac{Y}{n_w} \sin\theta_{max} \tag{22-a}$$

$$X_{max} = 0.0144Y \qquad \text{(32x lens)} \tag{22-b}$$

$$X_{max} = 0.0203Y \qquad \text{(50x lens)} \tag{22-c}$$

It should be pointed out that this analysis does not consider the effect of defraction which would modify the constants in Eqs. 22. The expressions are qualitatively correct, however, and the conclusion is that the field of view for the virtual image increases linearly with Y until the field of view of the lens or camera is reached.

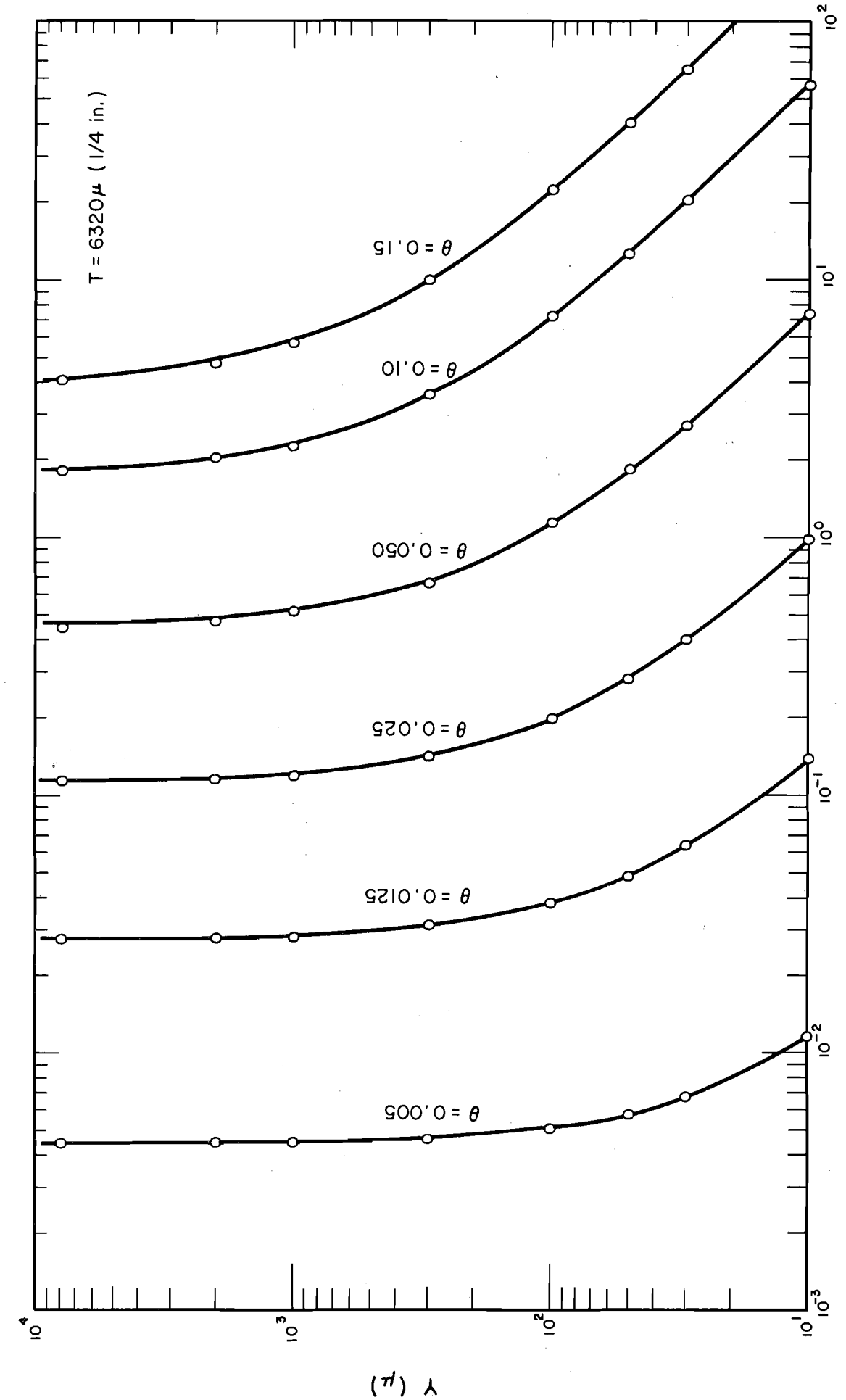

FIG. 7 EFFECT OF RAY ANGLES ON $x - x_v$

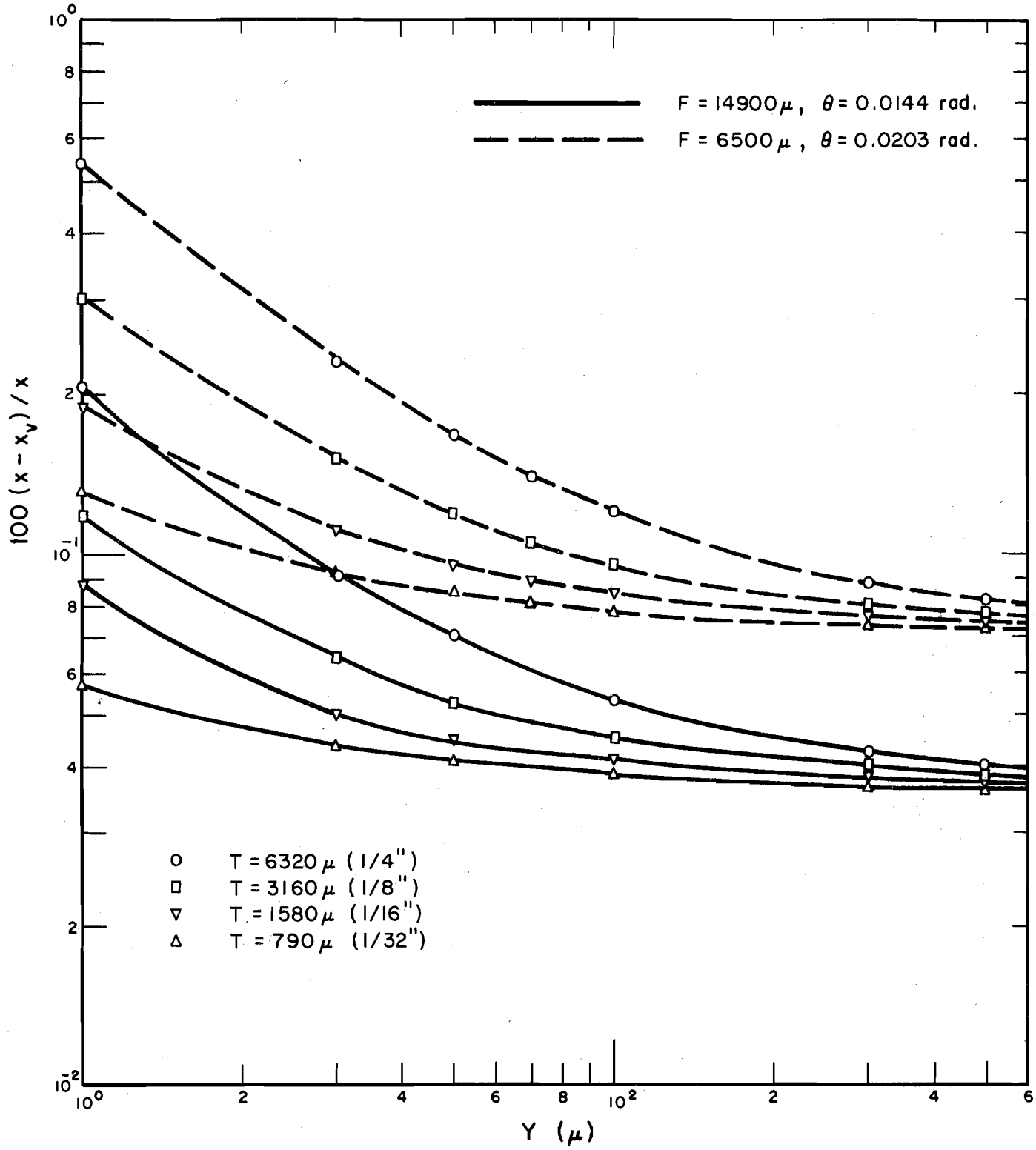

FIG. 8 EFFECT OF BOTTOM THICKNESS ON $x - x_v$

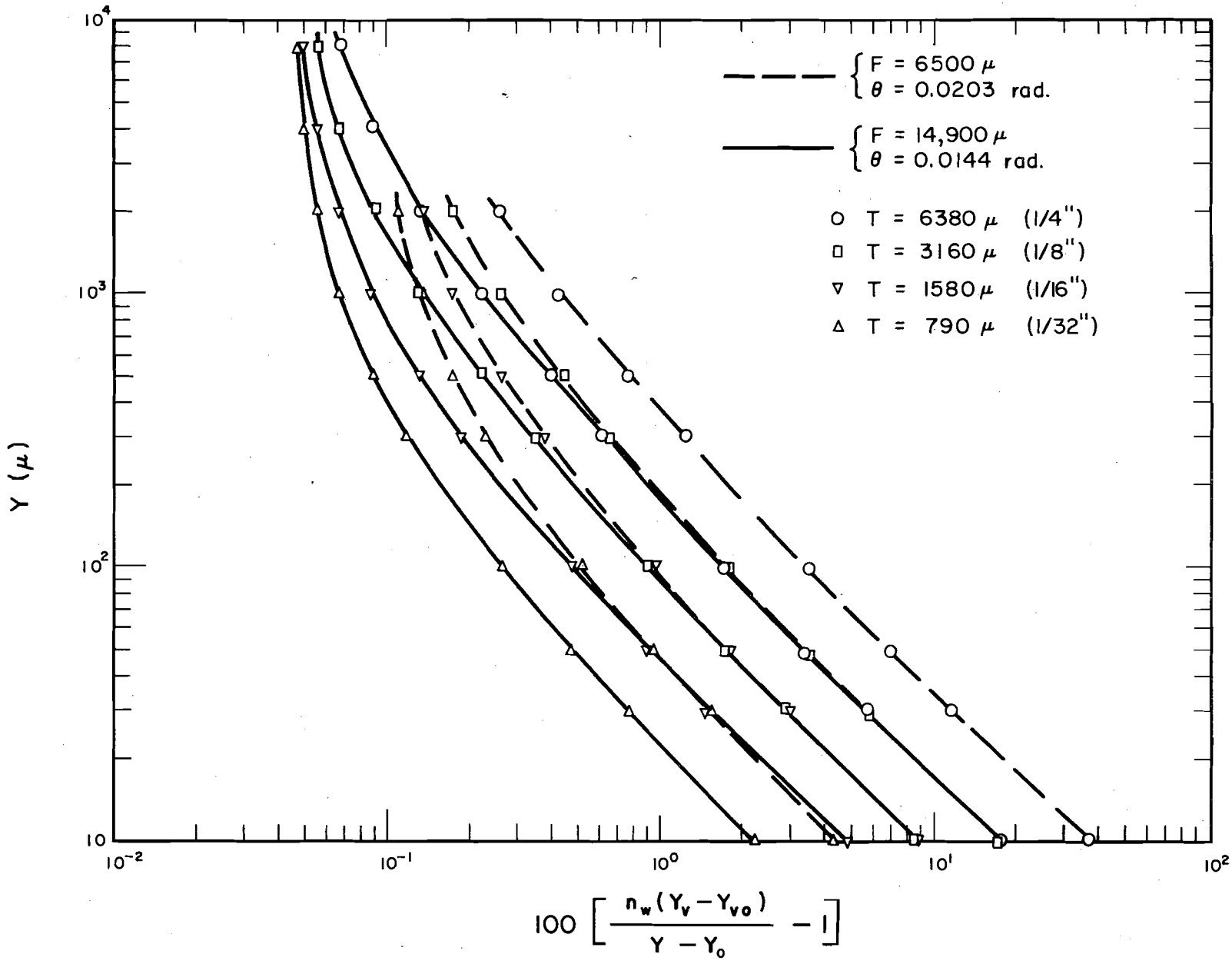

FIG. 9 EFFECT OF BOTTOM THICKNESS ON $Y_v - Y$

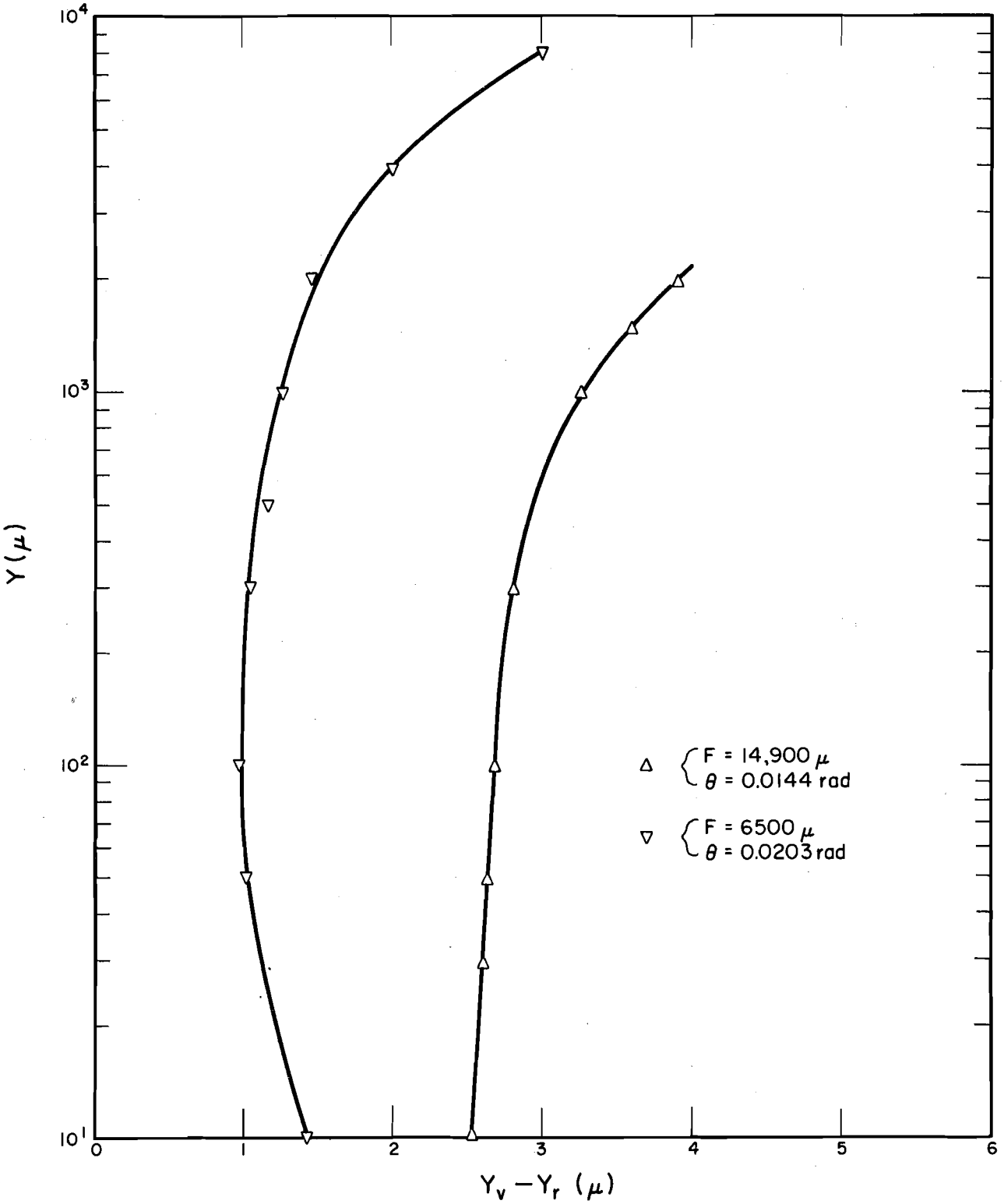

FIG. 10 EFFECT OF BOTTOM THICKNESS ON $Y_v - Y_r$

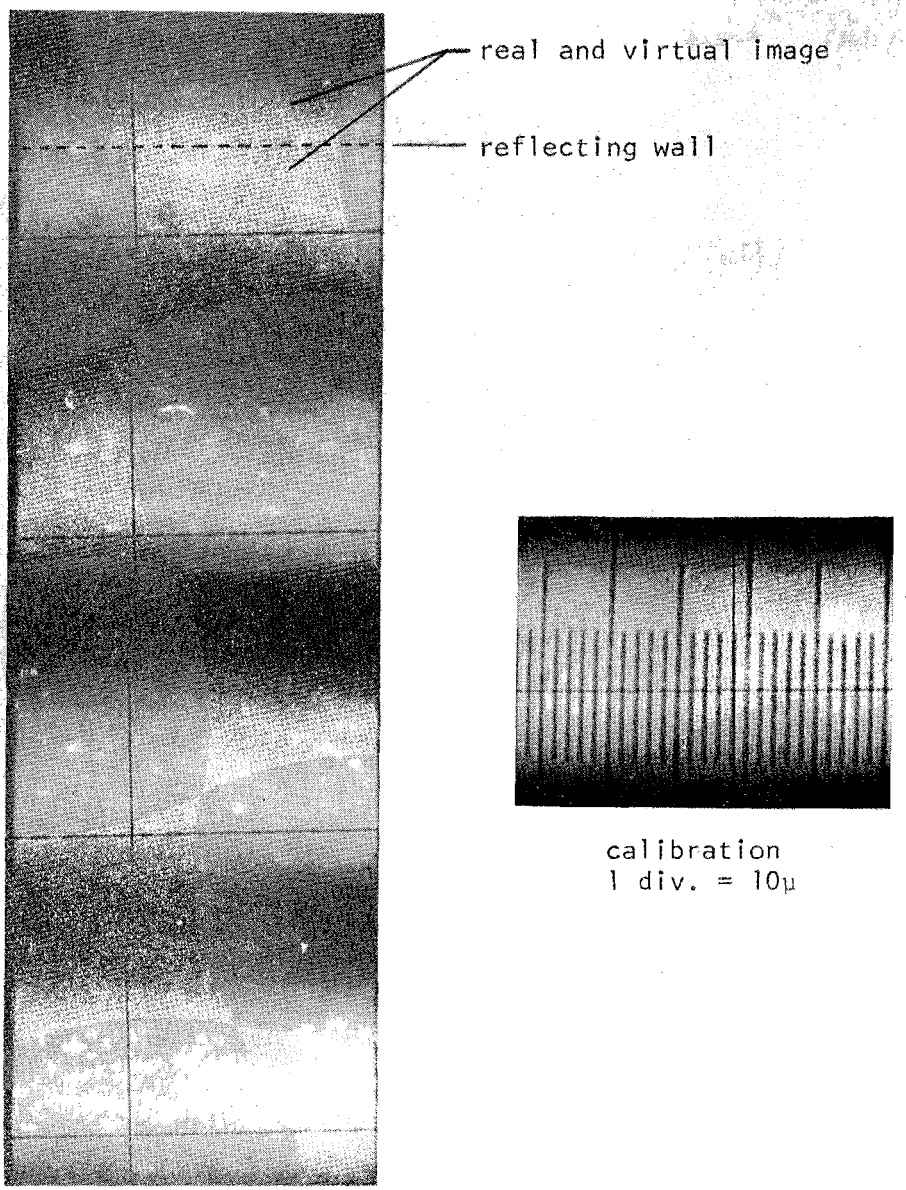

film speed ≈ 1000 frames/sec

Fig. 11 — Enlargement of Film of Particle Motion

4. RESULTS AND CONCLUSIONS

4.1 — Results

The results of this study are qualitative in nature due to the difficulty in obtaining sufficient light intensity to produce films containing sufficient particles to make data analysis feasible. Although the same light source was used successfully in the method described in WRC Research Report 13, the system which focused the light on the particle was different. In Report 13 a conventional darkfield condenser was used and positioned directly over the particle. This was not possible in this study due to the proximity of the particle to the wall. The lens system that was used was apparently not capable of focusing the light properly so that photographs could be taken. The particles were visible to the eye through the microscope but were not exposed in sufficient quantity on the film.

Given more time, support and experienced laboratory assistance this problem could certainly be overcome. However, recent developments in the field of surface hot film anemometer probes make it evident that there are better ways to investigate shear stress distribution around a wetted perimeter.

However, the method itself has great potential in boundary layer studies. For example, it provides a way of studying the flow around a hot wire or film anemometer and possibly making a primary calibration. Sublayer turbulence can be observed and measured and flow around roughness elements on the boundary can be observed.

The lighting problem was the only significant difficulty encountered. The method is generally superior to the real image method

described on WRC Report 13 because the uncertainty associated with the particle location has been removed. The distance from the wall can be determined directly from the film quite accurately as shown in Chapter 3. Of course there is still some uncertainty regarding the location with respect to the channel bottom due to the finite depth of field, however, this is not significant except very near the bottom where a high vertical velocity gradient exists. Away from the bottom the gradient across the depth of field is very small and probably is not significant.

4.2 — Conclusions

Based on this study the following conclusions can be made:

1. The most difficult experimental problem in adapting the image method is obtaining adequate lighting. The system used to focus the light on the particle is very important.

2. The image method overcomes the disadvantages of the parallel plane method since the distance of the particle from the wall can be determined directly from the film.

3. The image method can yield velocity information to within several microns of the wall. This is not possible using any type of velocity probe.

4. The amount of work needed to reduce the data is significant and probably is not justified if boundary shear stress information is the only result of interest. In this case other methods such as the hot film anemometer surface probe should be considered. However, if velocity data are of interest the method may be quite valuable.

REFERENCES

1. Wenzel, H. G. and Mathews, M. J., "Microscopic Determination of Boundary Shear and Sublayer Turbulence Characteristics in an Open Channel," University of Illinois Water Resources Center Report No. 13, Jan., 1968.

2. Chen, C. J. and Emrich, R. J., "Investigation of the Shock Tube Boundary Layer by a Tracer Method," Physics of Fluids, Vol. 6, No. 1, Jan., 1963.

3. Elrick, R. M. and Emrich, R. J., "Tracer Study of Pipe Flow Behavior to Within Two Micron of the Wall," Physics of Fluids, Vol. 9, No. 1, Jan., 1966.

4. Fage, A. and Townend, H.C.H.,"An Examination of Turbulent Flow with an Ultramicroscope," Proc. Royal Soc., Vol. 135, Ser. A, 1932.

5. Fage, A., "Turbulent Flow in a Circular Pipe," Philosophical Mag. Vol. 21, Ser. 17, 1936.

6. Vogelphol, G. and Mannesmann, D., "Flow Investigation with the Aid of the Ultramicroscope," NACA TM 1109 (Translation), 1946.

7. Fage, A. and Preston, J. H., "On Transition from Laminar to Turbulent Flow in the Boundary Layer," Proc. Royal Soc., Vol. 178, Ser. A, 1941.

8. Fage, A., "Studies of Boundary Layer Flow with a Fluid Motion Microscope," Nat'l. Phys. Lab., Teddington, Middlesex, Eng., 1955.

9. Bock, P. "Some Physical Aspects of Flow Near Surface," Trans. New York Aca. Sci., Ser. III, Vol. 25, 1963.

10. Vasuki, N. C., "A Dark Field Photographic Method for Measuring Velocity Profiles," M.S. Thesis, Univ. of Delaware, 1963.

11. Carver, C. E. and Nadolink, R. H., "Measurement of Laminar Velocity Profiles with Non-Newtonian Additives Using Photomicroscopy," Univ. of Mass. Fluid Mech. Lab. Tech. Report No. 1, Sept. 1965.

12. Carver, C. E. and Nadolink, R. H., "An Investigation of Velocity Profiles in the Laminar Sublayer with Non-Newtonian Additives Using High Speed Photomicroscopy," Univ. of Mass. Eng. Res. Inst. Report 69-3, May, 1969.